JOURNAL OF SPACECRAFT AND ROCKETS
Vol. 43, No. 5, September–October 2006

Optimization of Viscous Waveriders Derived from Axisymmetric Power-Law Blunt Body Flows

B. Mangin*
Centre National de la Recherche Scientifique, 45077 Orléans, France
R. Benay† and B. Chanetz‡
ONERA DAFE, 92190 Meudon, France
and
A. Chpoun§
Centre National de la Recherche Scientifique, 45077 Orléans, France

DOI: 10.2514/1.20079

A method based on a Euler code is used to study waveriders generated from the flowfield around cones or axisymmetric power-law blunt bodies. In the cone case, the results are compared with those given by the Taylor–Maccoll system and inviscid hypersonic small-disturbance theory. This last theory shows its limits at a Mach number of 5, for cone angles providing the best lift-to-drag ratios. In the axisymmetric power-law blunt body flows case, the optimization is led using a nonlinear simplex method to get the upper surface that enables the waverider to have the best lift-to-drag ratio, the thickness-to-length ratio being fixed. Compared with the cone-derived waverider, the proposed blunt-body-derived model allows a 20% gain in volume for near equal optimized lift-to-drag ratios.

Nomenclature

CDw	=	wave drag coefficient
Cf	=	friction coefficient
CL	=	lift coefficient
CmG	=	pitching moment coefficient at the center of volume
CP	=	center of pressure
CV	=	center of volume
D	=	total drag
D_f	=	friction drag
D_w	=	wave drag
$\mathrm{d}S$	=	triangular half-cell surface
H	=	shape factor
L	=	total lift
L_f	=	vertical component of the friction strain
L_w	=	waverider length
M	=	Mach number
Moz	=	pitching moment of the waverider at the nose of the reference body
n	=	power of the reference body
p	=	pressure
q	=	dynamic pressure
Reu	=	unitary Reynolds number
Ro	=	radial distance at $\varphi = 0$
Rs	=	shock radius in the base plane
Sp	=	planform surface area (on the z–x plane)
Sw	=	wetted surface area
V	=	volume
Xt	=	transition location
X	=	freestreamwise coordinate
Y	=	downward vertical coordinate
Z	=	spanwise coordinate
δ	=	cone angle or body thickness angle
η	=	volumetric coefficient. $\eta = V^{2/3}/S_p$
ρ	=	radius
$\rho 1$	=	radial distance at $\varphi = \phi l/3$
$\rho 2$	=	radial distance at $\varphi = 2\phi l/3$
ϕl	=	dihedral angle, defining the waverider width
φ	=	azimuthal angle

Subscript

∞	=	freestream
max	=	maximum

Received 15 September 2005; revision received 23 March 2006; accepted for publication 10 April 2006.

*Ph.D. Student, Laboratoire d'Aérothermique, 1C Avenue de la Recherche Scientifique; manginbo@yahoo.fr.
†Assignment/Theoretical Exploitation Head, 8 rue des Vertugadins.
‡Research Director, 8 rue des Vertugadins.
§Professor, Laboratoire d'Aérothermique, 1C Avenue de la Recherche Scientifique.

I. Introduction

PROJECTS about future hypersonic transport vehicles and the recent relevance of military hypersonic drones have led to a renewed interest in the waverider concept. This concept, providing interesting aerodynamic coefficients for a hypersonic vehicle, will contribute to fuel efficiency and may raise the economic viability of civil hypersonic transport aircraft. In the 1950s, confronted with the challenge of avoiding leakage due to shock standoff (for bodies with blunt noses), Nonweiler [1] found a method for defining hypersonic vehicle shapes that simultaneously solved this problem and allowed him to take into account the 3-D geometry in a simple way. Waveriders are generated by an inverse method: the undersurface is a stream surface of a known inviscid flow around a reference body after its refraction by the front shock (see Fig. 1). The leading edge is the intersection of a freestream surface (which provides the upper surface) and the shock created by the reference body. Leading-edge sharpness prevents leakage and so provides high lift-to-drag ratios (the compression zone is isolated by the shock). The undersurface being a stream surface, the waverider cruising at supersonic or hypersonic speeds creates the same shock wave as that due to the reference body and seems to be riding on top of this shock (thus its name). If the reference body is a wedge or an axisymmetric body, the flowfield will be two-dimensional.

High lift-to-drag ratios are very difficult to obtain at hypersonic speeds due to high wave drag and massive viscous effects. Kuchemann [2] exhibits an empirical correlation for $(L/D)_{\max}$ based on experiments:

$$(L/D)_{\max} = [4(M_\infty + 3)]/M_\infty$$

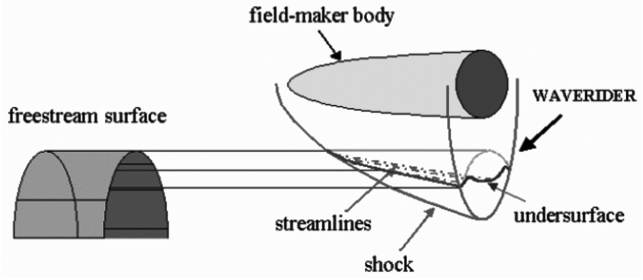

Fig. 1 Inverse method to create a waverider.

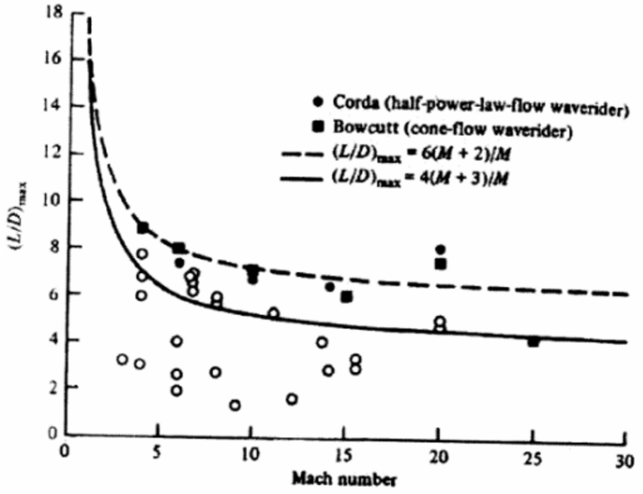

Fig. 2 Maximum lift-to-drag ratios (without base drag) vs. Mach number and empirical barriers.

(see Fig. 2). Studies lead by Corda et al. [3] and Bowcutt [4] show that waveriders break this barrier.

Cone-derived waveriders present better volumes than the wedge-derived ones because the concave streamlines are closer to the shock. Thus, waveriders' streamlined shapes were originally obtained from the flowfields around cones and wedges for their ease of calculation. If these profiles actually offered the desired good lift-to-drag ratios, on the other hand, they did not respond to the requirements in terms of useful volume vs. overall dimensions (the obtained profiles were very thin). Progress in numerical methods and increasing computer performances have allowed the field of possible generating shapes to enlarge. Waverider generation from the aerodynamic field calculated around blunt bodies, coupled with an optimization process, should better take into account both aerodynamic performance objectives and volume constraints. The goal is to improve the carrying capacity and to facilitate motor integration.

Blunt-body-derived waveriders are more voluminous because the streamlines are convex. Rasmussen and Brandes-Duncan [6] used hypersonic small-disturbance theory to study power-law blunt-body-derived waveriders. The nose profile was defined as a power of the streamwise coordinate. It was found that inviscid lift-to-drag ratio was maximal for a power n close to 0.7 and about 15% higher than in the conical case. In this study, a CFD Euler code is used to create blunt body flows and an optimization including viscous stresses evaluation is led. This optimization uses a nonlinear simplex method to get the upper surface that enables the waverider to have the best lift-to-drag ratio, the thickness-to-length ratio being fixed.

II. Creation of a Waverider

Presented next are the steps of a waverider creation and how the strains it undergoes are evaluated.

A. Steps

A waverider is considered as the forebody of an entire configuration and the base design is not considered. To accurately determine the flow around a blunt reference body, including the subsonic zone at the nose, where the method of characteristics is not applicable, the use of an Euler code is suitable. The hypersonic flowfields around the power-law axisymmetric body considered is thus obtained by use of the ONERA code FLU3M [7]. When the reference body is a cone, calculations are possible by two other means, one by solving the Taylor–Maccoll system and the other by use of hypersonic small-disturbance assumptions. The three methods have consequently been compared on this last configuration.

The cylindrical upper surface is defined by its cross section in a z–y plane (or in the corresponding ρ–φ plane when using polar coordinates) with Y as an even function of Z or ρ as an even function of φ. The leading edge is the intersection of this freestream surface and the shock created by the reference body. The undersurface is the stream surface starting from this curve in the 2-D or axisymmetric reference flow. Indeed, viscosity being neglected, a streamline can be considered as a solid wall on which the neighboring streamlines slip. As a result, the waverider will create the same shock as the reference body (Fig. 1).

Integrating static overpressures on the undersurface provides D_w (X component) and L (Y component). The upper surface being parallel to the freestream, its pressure is at freestream conditions so that there is no created drag or lift.

Wall shear stresses are evaluated by semiempirical means with the temperature reference method (see the Viscous Effects section). Their sum over the wetted surface provides D_f (X component), and a very small component opposed to the L_f. The base drag is not considered.

Some geometrical characteristics are calculated. In particular, the under and upper surface areas, the planform area (on the $Y = 0$ plane), and the volume are given (see [8]). The center of volume (i.e., the center of gravity for homogeneous waveriders) and the center of pressure (where aerodynamic moments are null) are computed too. The center of gravity is computed in the same manner as the volume: basic shapes as tetrahedron, pyramid, and regular prism are superimposed to form the volume confined between a cell of the wetted surface and a reference plane $Y = 0$. The shift between the undersurface and upper surface shapes provides the waverider.

B. Flowfields

Two kinds of axisymmetric flowfields are considered following the type of reference body (a cone or a blunt power-law axisymmetric body).

1. Conical Flowfield

Aerodynamic flowfields on cones have been calculated using the Euler code and two other methods: the first solves the Taylor–Maccoll system derived from the Euler equations with conical assumption, and the second is based on the hypersonic small-disturbance theory.

Conical assumption is that polar angle is the only variable (axisymmetric field and no length scale). So Euler equations can take the following form of the Taylor–Maccoll system [9]:

$$u' = v; \qquad v' = \frac{u[v^2 - 2(a/a^*)^2] - v(a/a^*)^2 \cot\theta}{(a/a^*)^2 - v^2}$$

with u and v are polar components of the speed nondimensionalized by a^*, the freestream critical speed of sound. Flow conditions downstream of the shock are obtained, thanks to attached-shock relations for a perfect gas. The Taylor–Maccoll system is solved by iterations using a fourth-order Runge–Kutta algorithm. A conical flowfield is pictured in Fig. 3.

Hypersonic small-disturbance theory assumption [10,11] enables us to solve the Taylor–Maccoll system analytically. It requires the assumption that the cone is slender enough and the freestream Mach number high enough to apply small angle hypothesis. The

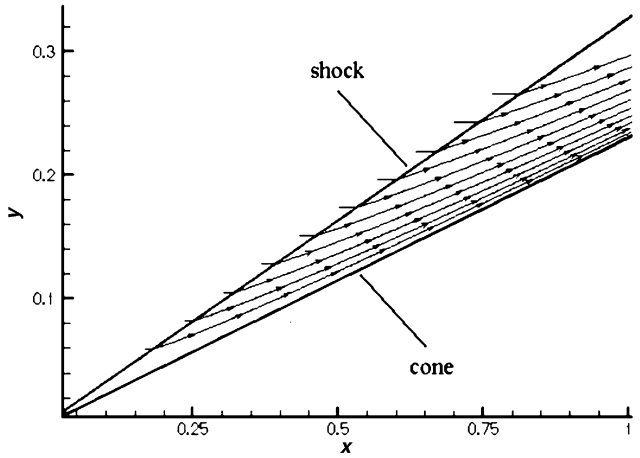

Fig. 3 Streamlines of a conical flowfield (Taylor–Maccoll method).

orthoradial speed component is then

$$v/V_\infty = -\theta[1 - \delta^2/\theta^2] = u'/V_\infty$$

The shock angle-to-cone angle ratio is given by the similarity relation

$$\sigma = \beta/\delta = [(\gamma + 1)/2 + 1/K_\delta^2]^{1/2}$$

with $K_\delta = M_\infty.\delta$. The undersurface is created from the mass flow conservation between it and the cone and from the hypothesis of a constant density downstream of the shock.

2. Power-Law Bodies Flowfields

Rasmussen and Brandes-Duncan [6] used a hypersonic small-disturbance theory to study power-law blunt-body-derived waveriders. In this case, the equation of the reference body in an x–y plane is $Y = A.X^n$. Idealized waveriders (half of the reference body as the undersurface and two flat planes as the upper surface) were studied with n varying between 0.5 to 1. Viscous strains not being taken into account, it was found that lift-to-drag ratio was maximal for n close to 0.7 (this maximum is about 15% higher than in the conical case). Moreover, streamlines around blunt power-law bodies enable us to create waveriders with convex undersurfaces. Hence volume increase appears as a supplementary advantage. The Euler code was used to create aerodynamic flowfields around blunt power-law bodies. The length of the body is 1.0 m and the waverider length is 0.1 m. The thickness angle being δ, the blunt body is defined as

$$(Y = \tan(\delta).X^n)$$

This Euler version of the ONERA FLU3M [7] code uses a Roe scheme on structured monozone grids. No Harten correction was needed. The two-dimensional grid is designed to obtain high point density around the body (see Fig. 4).

Grid convergence is guaranteed by the comparison of the results obtained with various mesh definitions. The final grid definition has 480 points in I (along the wall) and 110 in J (normal to the wall) coordinates (spatial convergence of the calculation is obtained with less points, especially along I coordinates but this high definition is needed to obtain smooth streamlines and a thin shock).

C. Leading-Edge Design

The upper surface being cylindrical, its projection in a y–z plane is also the leading-edge projection. In this study, it is defined by a polynom function

$$Y = f(Z) \text{ or } \rho = f(\varphi)$$

(see Fig. 5). The first kind of parameterization has only been considered in the case of cone-derived waveriders. In this case, a second-degree polynom gives what is called parabolic-top waveriders (see [10]). The leading-edge projection is the parabola

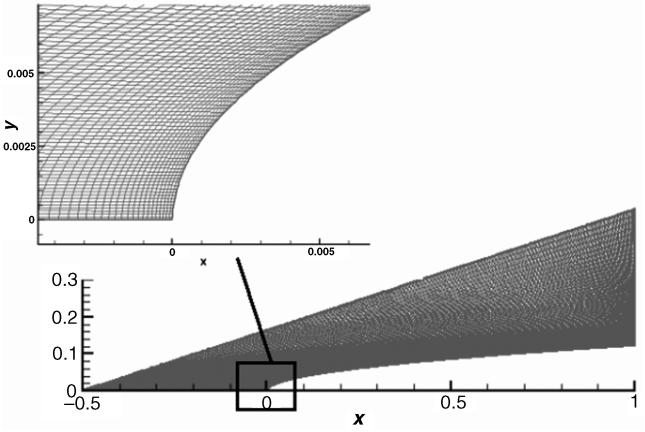

Fig. 4 Grid around a power-law body ($\delta = 5$ deg, $n = 0.5$).

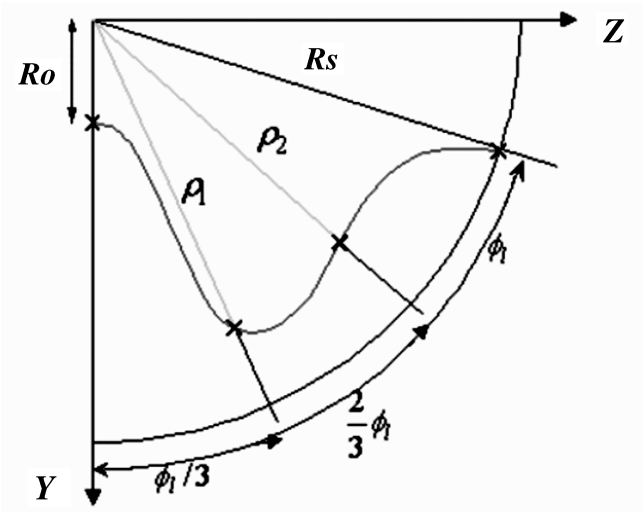

Fig. 5 A symmetric sixth-degree upper surface and its parameters.

that passes through the points 0, Ro and $Rs.\sin\Phi l$, and $Rs.\cos\Phi l$ (of course the shock projection is a circle in this axisymmetric case).

In a more general optimization process, the polynom is the even Lagrangian sixth-degree polynom $\rho = f(\varphi)$ that passes through the points 0, Ro; $\rho 1, \varphi 1$; $\rho 2, \varphi 2$; and Rs, Φl with $\varphi 1 = \Phi l/3$ and $\varphi 2 = 2/3\Phi l$. The polar representation $\rho = f(\varphi)$ ensures a single radial position of the leading-edge projection for a given φ.

D. Viscous Effects

Viscous stresses are evaluated using two integral methods based on empirical formulations of the friction coefficient: the Eckert reference temperature [12] method and the Michel–Cousteix method [12], considering uniform and nonuniform external flowfields, respectively. In the shock downstream area, the pressure increases along a streamline in the case of a conical flow, whereas it decreases in the case of a power-law blunt body flow. The two methods have been used to evaluate these variations effects on viscous stresses.

Transition location is evaluated thanks to experimental results on slender cones [13]. If the waverider length is lower than the transition location, the friction coefficient is given by the corrected well-known Blasius formula

$$Cf(x) = (0.664/\sqrt{Re_x})f$$

with the local Reynolds number $Re_x = \rho_e u_e x/\mu_e$, and f, a correction factor which enables us to apply incompressible Blasius formula to supersonic flowfields, given by

$$f = \sqrt{\rho_r \mu_r/\rho_e \mu_e} = \sqrt{T_e \mu_r/T_r \mu_e}$$

Table 1 Friction evaluation coefficients

	Laminar	Turbulent
k	0.2205	0.0086
m	1	1/5
Hi	2.6	1.4
α	0.667	0.4
β	2.9	1.22

where the reference temperature Tr is Monaghan's temperature [12]. In the turbulent case (with the assumption that transition location is quite lower than the waverider length), the friction coefficient is given by

$$Cf(x) = [0.0368/(Re_x)^{1/6}]f$$

where the compressible correction factor is

$$f = (\rho_r/\rho_e)^{5/6}(\mu_r/\mu_e)^{1/6} = (T_e/T_r)^{5/6}(\mu_r/\mu_e)^{1/6}$$

The Michel–Cousteix method deals with the integration of the von Kármán equation:

$$Cf/2 = (\mathrm{d}\theta/\mathrm{d}x) + \theta\{[(H+2)/U_e](\mathrm{d}U_e/\mathrm{d}x) + (1/\rho_e)(\mathrm{d}\rho_e/\mathrm{d}x) + (1/R)(\mathrm{d}R/\mathrm{d}x)\}$$

where θ is the momentum thickness, H the shape factor, and R the distance to the symmetry axis ($R = 1$ for two-dimensional cases). $Cf/2$ and H are supposed to check the following rules relative to the flat plate case:

$$Cf/2 = k.g/Re_\theta^m$$

(with k and m corresponding to the laminar or turbulent case, see Table 1) and

$$H = H_i + \alpha.M_e^2 + \beta(T_p - T_f/T_e)$$

(see the Nomenclature). The compressible correction factor is g. The solution θ checks:

$$[F.E(\theta.R)^{m+1}]_x = [F.E(\theta.R)^{m+1}]_{x=x1} + \int_{x1}^{x} \frac{g.F.E.R^{m+1}}{(\rho_e U_e/\mu_e)^m}\mathrm{d}t$$

where t is the curb abscissa,

$$E(x) = \exp\left[\beta.(m+1)\int_{x1}^{x}\frac{T_p - T_f}{T_e}.\frac{\mathrm{d}U_e}{U_e}\right]$$

and

$$F(x) = [U_e^{Hi+2}.\rho_e^{1-\alpha}]^{m+1}$$

Results from the two methods have been compared locally with friction coefficient and globally with friction drag. The reference skin friction is that of the first method. The relative shift between friction coefficients is never greater than 5%, as for the conical case. The resulting friction drag difference is lower than 2%, showing that local shifts between the two methods have weak effects on it. Hence the reference temperature method was used in the optimization process.

E. Stresses

Each generating streamline has the same number of points (100 points for the 100 streamlines to ensure stresses convergence) giving a 100×100 grid that structures the undersurface (defined by indices I and J). The wave drag and lift of each cell are the components of the average pressure strain multiplied by the cell area. For each cell, the average component of the strain due to the Cf parallel to the local inviscid speed multiplied by the cell area gives its contribution to the drag. By summing on all the cells, the lift-to-drag ratio is given by Eq. (1):

$$\frac{L}{D} = \frac{L + L_f}{D_w + D_f} = \frac{\iint_{SWC}(p - p_\infty)\mathrm{d}\boldsymbol{S}.\boldsymbol{e}_{y'} + q_\infty \iint_{SW} Cf.\mathrm{d}S\boldsymbol{te}_{y'}}{\iint_{SWC}(p - p_\infty)\mathrm{d}\boldsymbol{S}.\boldsymbol{e}_{x'} + q_\infty \iint_{SW} Cf.\mathrm{d}S\boldsymbol{te}_{x'}} \quad (1)$$

with $\boldsymbol{e}_{y'} = \boldsymbol{e}_y$. In the small-disturbance-based method, pressure forces are evaluated thanks to analytic formulas [10,11] derived from a momentum flux balance.

III. Optimization

The aim of this work is to find waveriders with the highest lift-to-drag ratios able to perform useful tasks (e.g., a sufficient volume). A first study is made to understand the parameters influence on aerodynamic and geometric characteristics in the particular case of the cone-derived waveriders with parabolic tops. Then a more general optimization process based on a nonlinear simplex method is used to find the leading edge providing the best lift-to-drag ratio for waveriders created from power-law body generated flowfields.

A. Parameters Influences

The first type of parameters defining a waverider are those relative to the reference body. In the conical case, it is only the cone angle δ. In the case of a power-law blunt body, these parameters are the thickness-to-length ratio $\tan(\delta)$ and the power n in the reference body defining equation $y = \tan(\delta)x^n$. The second type of parameters are the waverider length Lw and the previously defined Ro, $\rho 1$, $\rho 2$, and Φl. When the last four parameters increase, the undersurface streamlines go away from the reference body, and so are less deflected, hence the waverider is thinner (pressure strains decrease). But when Ro and Φl increase, the width and the wetted area also increase and so does the viscous strain. There is an equilibrium to find between the thickest waverider, which is the half-reference-body ($Ro \to 0$), and the flat plate (Ro, 1, $\rho 1$, and $\rho 2 \to$ infinity). Indeed, for thick waveriders, the friction drag can be negligible in front of the wave drag and for thin waveriders the contrary can happen. Hence, with Ro, $\rho 1$, and $\rho 2$ being fixed, there is a particular reference body thickness-to-length ratio that provides the highest lift-to-drag ratio (see the optimal cone angle in Fig. 6).

B. Nonlinear Simplex Optimization Process

Most optimization schemes are based on variational methods that require analytical descriptions. However, a nonlinear simplex method for function minimization by Nelder and Mead [14] enables us to converge toward the best configuration just by evaluating the function to minimize in a pool of configurations. Here it is considered for minimizing the inverse of the lift-to-drag ratio. With n parameters, the simplex is made of $n + 1$ points, a point or configuration representing a waverider. At each step, the worst configuration (with the highest value) is eliminated and replaced by a

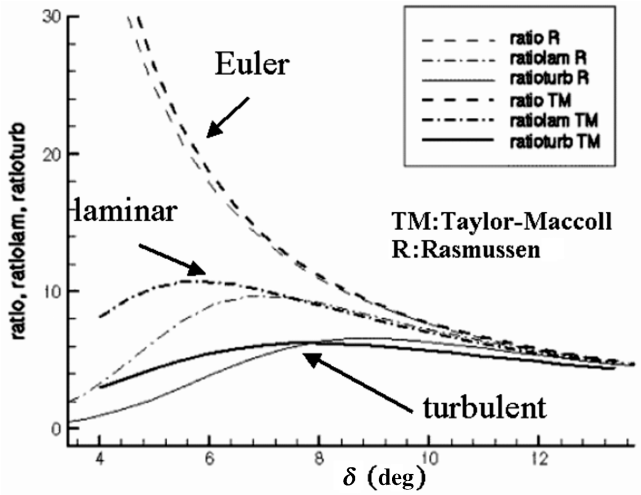

Fig. 6 Lift-to-drag ratios vs. cone angle (Taylor–Maccoll and Rasmussen methods).

Table 2 Flow conditions

	Case 1	Case 2
Mach number	5	4.96
Total pressure (Pa)	32e5	8.5e5
Total temperature (K)	500	453
Reu (m-1)	40e6	12.66e6
Rext	4.78e6	2.75E6
Xt (m)	0.12	0.21
Length (m)	0.25	0.1

new one: it is the image of the worst one by the reflection through the center (or average configuration) of the others. If the function at this point has the lowest value, an expansion occurs: this point is replaced by the image of the last center by the reflection through it. If the function at this point has the highest value, a contraction occurs: this point is replaced by the center of itself and the last center. Finally the process converges to the best configuration vicinity.

In this study, the simplex method was not applied directly with all the parameters. The reference body parameters δ and n cannot take all the values because each couple corresponds to a mesh. Indeed, automation of the entire process (mesh creation, calculus, and optimization with the remaining parameters) has not been undertaken because of the complexity of the chain and the subsequent enormous time required by a step. The method resembles the optimization of cone-derived waveriders lead by Bowcutt et al. [4], where the simplex method was used for a fixed shock angle (hence fixed cone angle), the final best waverider being the best of the bests obtained for each of the studied shock angles.

Two different freestream conditions (see Table 2) have been studied. Case 1 (ONERA Meudon R2-Ch wind tunnel) has been chosen for comparing the different methods in the parabolic-top case and case 2 (CNRS Orléans SH2 wind tunnel) corresponds to the optimization part. In the second case, the waverider has a totally laminar boundary layer. The first and second conditions, respectively, were applied on waveriders whose length was 0.25 and 0.1 m, respectively. Experiments led on slender cones furnished a correlation between unitary Reynolds number and transition Reynolds number (see [13] and Table 2). Hence it appears that the waverider tested in the second case would have a laminar boundary layer on its first half and a turbulent one on its second. Meanwhile, it is considered that the boundary layer is totally turbulent. (Friction strains have been overevaluated rather than considering a nonprecise transition location.)

IV. Results

A. Comparison of Taylor–Maccoll/Small Disturbances

It is known that the hypersonic small-disturbance theory (which will be called the Rasmussen method) works for small cone angles (less than 5 deg) and for high Mach numbers (greater than 10). Meanwhile results for a Mach number of 3 can be seen in the literature. To appreciate how it performs at Mach 5 with the considered cone angles, its results are compared with those given by Taylor–Maccoll calculations in the particular case of cone-derived waveriders with flat upper surfaces.

Each method allows its own determination of the undersurface geometry. In each case, strains are evaluated by the previously defined method. Ro being fixed ($Ro/Lw = 0.2$), in Fig. 6 we first compare lift-to-drag ratio evolutions vs. the cone angle given by the two methods. Lift-to-drag ratios are paradoxically different for lower cone angles. This shift, which can be seen when the viscosity is neglected, is amplified in the laminar and turbulent cases. This means that waverider geometries do not coincide. Indeed, for $\delta = 5$ deg, there is a non-negligible difference between the stream surfaces given by the two methods, although these are very close for $\delta = 12.95$ deg. (In Fig. 7 the undersurfaces are represented in reversed position relative to the ground by their projection in various transverse cutting planes.)

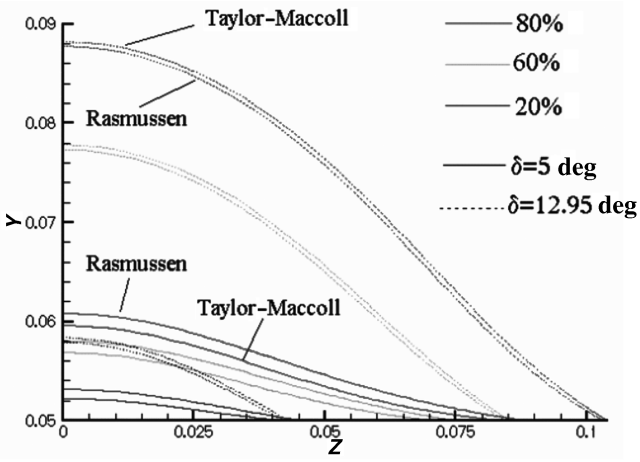

Fig. 7 Reversed undersurfaces in transverse cutting planes *Y*-*Z*.

The geometry shift is due to the fact that K must be high enough: according to Anderson [15], K must be higher than 0.5 and 1.5, respectively, for δ equal to 5 and 20 deg, respectively, corresponding to a Mach number higher than 5.73 and 4.30, respectively. In the present study, the Mach number is too low for δ less than 10 deg.

Moreover, the similarity relation provides shock angles whose relative shifts compared with Taylor–Maccoll results reach 4% (0.5 deg) for $\delta = 5$ deg. This explains why the hypersonic small-disturbances theory has not been used to study Mach 5 power-law body derived waveriders.

These results look like those of the flat plate under incidence (curves passing from pure skin friction at zero incidence to a pure wave drag at high incidence, crossing a maximum between the two states). All the curves are the same if the cone angle is greater than 13 deg, because friction strains are negligible compared with pressure strains, and shock angles are close.

B. Comparison of Taylor–Maccoll vs. Euler Calculations

The ONERA code FLU3M has been used to obtain the flowfields around power-law blunt bodies. Specific subroutines such as a shock localizer and a streamlines extractor have been implemented to create waveriders. The results given by the use of Taylor–Maccoll equations are compared with those of the Euler-code-based method.

A difference between these two methods can emerge when looking at the shock localization. Indeed, the Taylor–Maccoll method fits an infinitely thin shock whereas the Euler-code-based method creates a shock that smears over several grid points. Lobbia and Suzuki [16] encountered this problem with a drag shift of 13% and a lift shift of 22% between a 3-D Euler-code-based method and Taylor–Maccoll for a 10 deg cone. The use of a 3-D code prevented them from excessively increasing the number of points to thin the shock.

In our study, shock capturing consists of localizing the maximal pressure first derivative (between two neighboring grid points labeled as N and $N + 1$) of each gridline (in the I or J direction). The shock is considered as the curve passing through the middle of the intervals joining calculation points between which the pressure variation is maximal. Then the "ladder" curve is smoothed.

For a cone angle equal to 12.95 deg and Ro/Lw equal to 0.2, waveriders with a flat upper surface are obtained by using either of the two methods. Strains are very close, relative differences being lower than 4% (see Table 3). The aerodynamic coefficients are related to the wetted surface area. Geometries are very close too.

These results validate the Euler-code-based method to create waveriders. It will be used to create power-law blunt-body-derived waveriders.

C. Cone-Derived Waveriders with Parabolic Tops

The influence of parameters on aerodynamic and geometric characteristics will be pictured in the particular case of cone-derived

Table 3 Waveriders characteristics (Taylor–Maccoll/FLU3M)

$Lw = 0.25$ m, $Ro/Lw = 0.2$, $\delta = 12.95$ deg	Taylor–Maccoll	FLU3M	ε (%)
CDw	1.031E-02	0.991E-02	3.88
CL	5.334E-02	5.176E-02	2.96
Wetted surface area (m2)	7.634E-02	7.625E-02	0.12
Lift-to-drag ratio	5.175	5.231	1.18

waveriders with parabolic tops. The flowfield conditions are those of case 1. The definition of the leading-edge/upper-surface projection in a transverse y–z plane is described by $Y = A.Z + Ro$, with A chosen to enable the curve to pass through the point ($Rs \sin \Phi l$, $Rs. \cos \Phi l$). The three parameters defining these waveriders are the cone angle δ, Ro, and Φl.

Studied parameters lie in the range 4–10 deg for δ and in the range 10–80 deg for Φl. The minimum value of Ro needed to ensure the leading-edge projection to be φ-single valued depends on the first two parameters:

$$Ro > Rs.\,\mathbf{cos}(\Phi l)/2$$

If the obtained lift-to-drag ratios are pictured in the 3-D parameter space, it appears that lift-to-drag ratios are the highest in a curved tube, the axis of which is parallel to the Ro axis. This tube is symmetrically cut by the plane $\delta = 9.2\,\mathbf{deg}$ pictured in Fig. 8 (it corresponds to the previously evidenced optimal cone angle). For a ratio Ro/Lw greater than 0.04 (Ro higher than 1 cm for $Lw = 0.25$ **m**), the best lift-to-drag ratios lie in the zone included between the two curves corresponding, respectively, to waveriders as long as wide (the lower one, solid line) and waveriders with flat upper surfaces (the highest one, dotted line). This means that the best waveriders are slightly wider than long and have a convex upper surface. The best waverider with $Ro/Lw = 2.68$ ($Ro = 0.67$ **m**) is obtained for $\Phi l = 12.5\,\mathbf{deg}$, giving a lift-to-drag ratio equal to 6.53 and a width-to-length ratio equal to 1.28. This waverider is not very useful because it is too thin to carry loads (Ro is high, see Fig. 8, bottom right).

More useful and thicker waveriders are obtained with lower Ro. A waverider whose thickness-to-length ratio is equal to 0.1 corresponds to a ratio Ro/Lw equal to 0.8 ($Ro = 0.2$ m). In this case, the highest lift-to-drag ratio is equal to 6.43 and is obtained with $\Phi l = 29.4$ deg (see Fig. 9, bottom left). The asymptotic shape of a cone appears in the undersurface profile.

The volume distribution is pictured in Fig. 10 and shows that the most voluminous waverider is the one shown in Fig. 9, top right. The volume and the lift-to-drag ratio of this body are, respectively, equal to 4.89e-3 m^3 and 5.95. Its volume is due to its very high aspect ratio. It is obvious that such a body is out of aircraft applications. Practical reasons lead, therefore, to consider the body represented at the bottom left of Fig. 9, with a volume of 3.94e-4 m^3 and a lift-to-drag ratio of 6.43, as optimal. The optimization just performed of a cone-derived waverider, with a parabolic definition of the upper surface, was able to be led simply by a close inspection of the numerous performed calculations. In the case of less simple definitions of the upper surfaces, the optimization will require the use of a more improved technique.

D. Optimized Power-Law Blunt-Body-Derived Waveriders

The only waveriders considered in the optimization process are those with a thickness-to-length ratio equal to 0.1. Ro is chosen to ensure this condition and it is checked that it is high enough to be supersonic after the shock. This last condition is necessary for the shock wave to be attached to the leading edge: if it is not the case, the inverse method cannot be applied. The length of the reference bodies is 1 m.

The optimization process consists of searching the best shape for the upper surface of the body. The function to minimize is the inverse of the lift-to-drag ratio. The simplex process should have been applied to 24 undersurface geometries. These surfaces are generated by the streamlines of the Euler flowfields around reference bodies defined by $n = 0.5$, 0.6, 0.7, 0.8, 0.9, and 1.0 and $\delta = 3$, 5, 7, and 9 deg. We recall that the cases $n = 1$ are cones and the length of the reference body is 1 m. The particular reference bodies corresponding to $\delta = 3$ deg, $n = 0.8, 0.9$, and 1.0 and $\delta = 5$ deg, $n = 1.0$ were too slender to create waveriders as thick as a tenth of their length. Consequently, the simplex process was applied to the 20 remaining

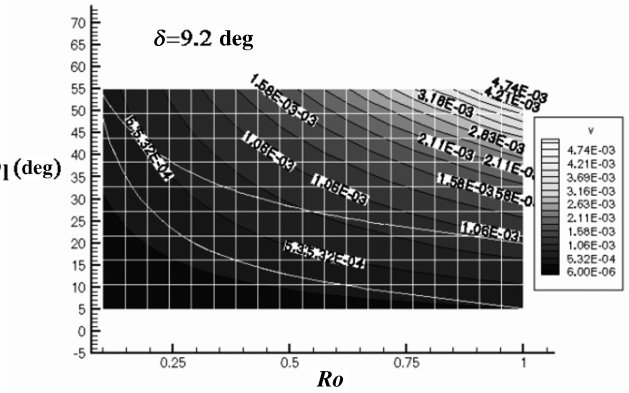

Fig. 9 Volume of conical-derived waveriders with parabolic tops (turbulent case, $\delta = 9.2\,\mathbf{deg}$).

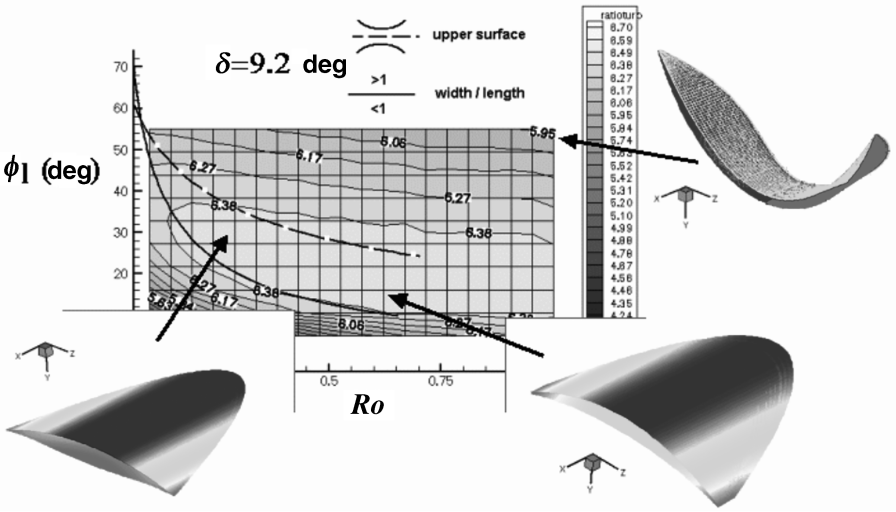

Fig. 8 Lift-to-drag ratio of conical-derived waveriders with parabolic tops (turbulent case, $Lw = 0.25$ m, $\delta = 9.2\,\mathbf{deg}$).

flowfields. The upstream conditions are those of case 2, assuming laminar boundary layers. For each case, Ro being fixed, the parameters are the width of dihedral angle Φl, and the distances of $\rho 1$ and $\rho 2$. One hundred simplex steps were generally necessary to accurately approach the minimum.

1. *Influence of the Reference Body Shape on Optimal Characteristics*

Fig. 10 shows the bases of the optimal waveriders obtained for all the studied reference bodies. In every case $\rho 1$, $\rho 2$, and Ro are close, and lift-to-drag ratios are higher than the empirical barrier (6.4). When Ro increases, the width of the optimal waveriders increases, but Φl decreases to limit the wetted surface area. The distance $\rho 2$ increases less than $\rho 1$ so that waveriders become more and more like a reversed W, which we called a *two-bump* configuration. The lift-to-drag distribution of these optimal waveriders is pictured in Fig. 11. The highest lift-to-drag ratio is obtained for the thickest reference body ($\delta = 9$ deg) with the lowest power ($n = 0.5$) and just reaches 7. It can be seen in Fig. 10 that it corresponds to a waverider wider than long (reminder that $Lw = 0.1$ m), which is an unpractical leading edge kind of waverider (the widest). Optimal waveriders that are longer than wide or slightly as long as wide are the ones in the outlined square in Fig. 10 and above the solid line in Fig. 11. If the waveriders that are wider than long are not to be considered, the best practical waverider is the one of the case $\delta = 7$ deg, $n = 0.7$. Note that the friction drag varies from 30% (slender reference bodies) to 60% (thicker reference bodies) of the total drag. Indeed, the base area increases with increasing reference body thickness, and the inviscid lift-to-drag ratio consequently decreases. For the case $\delta = 7$ deg, $n = 0.7$, the friction drag is 35% of the total drag (i.e., the wave drag is twice the friction drag). The volume-to-Lw [10] ratio distribution is pictured in Fig. 12. The highest volume is obtained for the case $\delta = 9$ deg, $n = 0.5$. As for the parabolic-top cone-derived waveriders, the volume is due to the width of the waverider (high Ro implies high shock radius). All the volumetric coefficients are close to 0.26 except for the case $\delta = 3$ deg, $n = 0.6$, where it is about 0.72. It can be seen in Figs. 10 and 13 that close optimal upper surfaces correspond to close values of Ro. Two optimal waveriders, the upper surfaces of which are close, are compared in the following section to consider the effect of the reference body on the lift-to-drag ratio and the volume.

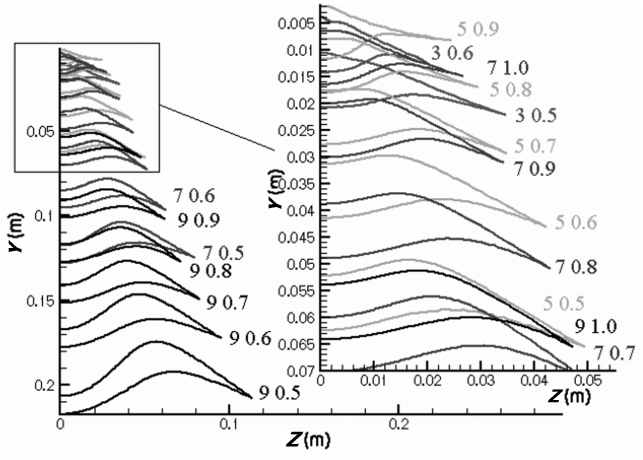

Fig. 10 Base view of optimal waveriders ($Lw = 0.1$ m).

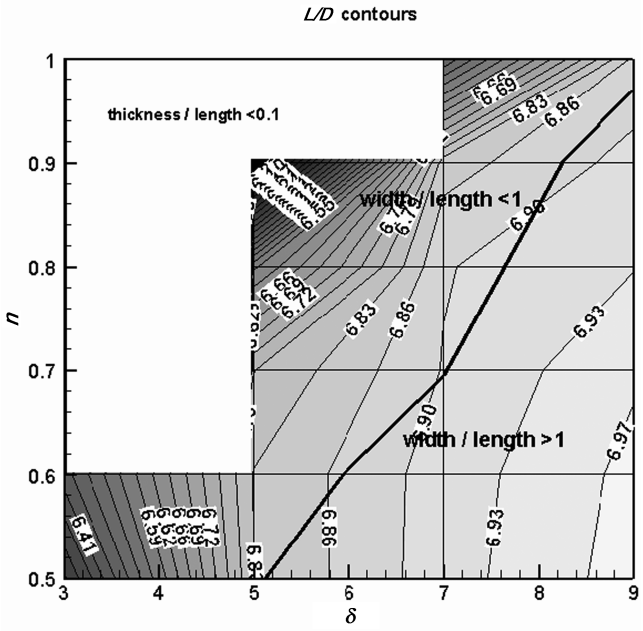

Fig. 11 Lift-to-drag ratio of the optimal waveriders.

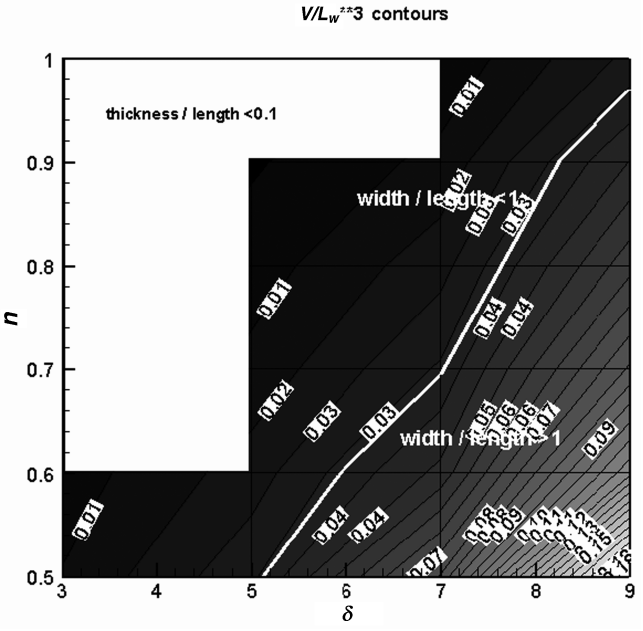

Fig. 12 Volume of the optimal waveriders.

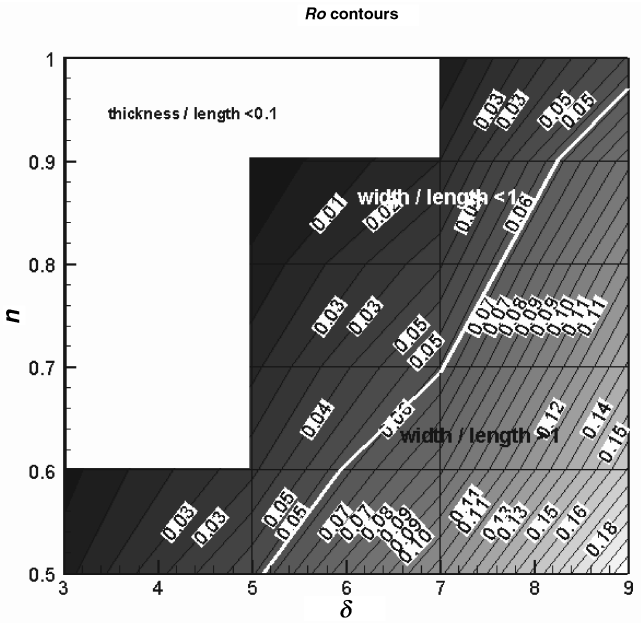

Fig. 13 Ro of the optimal waveriders.

Table 4 Optimized waveriders characteristics

Thickness-to-length ratio = 0.1	$\delta = 7$ deg, $n = 1.0$	$\delta = 7$ deg, $n = 0.7$	$\delta = 9$ deg, $n = 1.0$
Ro (m)	6.50e-3	0.060	0.054
$\rho 1$ (m)	7.00e-3	0.059	0.054
$\rho 2$ (m)	9.47e-3	0.062	0.057
ϕl (°)	60.72	34.98	35.69
Dw/D (%)	50.0	65.1	65.6
Lift-to-drag ratio	6.45	6.90	6.87
Volumetric coefficient	0.264	0.266	0.261

2. Toward an Optimal Shape

By considering not only lift-to-drag ratio but also the carrying capacity of the body (its volume), the two most interesting configurations, $\delta = 7$ deg, $n = 0.7$ and $\delta = 9$ deg, $n = 1.0$, are shown in Table 4. A synthetic representation of the geometries is given in Fig. 14. The configurations $\delta = 7$ deg, $n = 0.7$ and $\delta = 9$ deg, $n = 1.0$ are close, but the first one, generated with a blunt reference body, presents a slightly higher lift-to-drag ratio of 6.90 instead of 6.87. The volume increase from $\delta = 9$ deg, $n = 1.0$ to the close blunt-body-derived configuration reaches 21%. The cone-derived case $\delta = 7$ deg, $n = 1.0$, whose shape is more classical than the two others, is added in Table 4 and in Fig. 14 for comparison. It illustrates the two kinds of geometries obtained in our optimization process. As a main result, the two-bump configuration has constantly appeared as the most interesting one. It is to be noticed that the three configurations overpass the empirical barrier of lift-to-drag ratios equal to 6.4.

A higher volume being obtained in the case of the two-bump configurations, we see clearly that, with respect to our criterion of maximum volume + maximum lift-to-drag ratio, the blunt body generated, $\delta = 7$ deg, $n = 0.7$, must be retained at the end of the process.

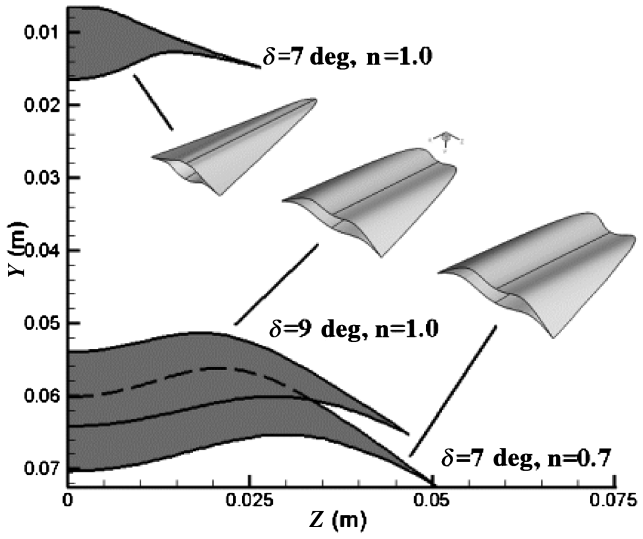

Fig. 14 Base view of three optimal waveriders.

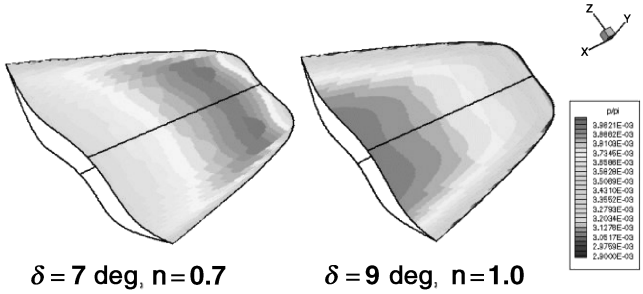

Fig. 15 Pressure distribution at the undersurface ($\delta = 7$ deg, $n = 0.7$) and ($\delta = 9$ deg, $n = 1.0$).

Table 5 Stability analysis of the cases $\delta = 7$ deg, $n = 0.7$ and $\delta = 9$ deg, $n = 1.0$

	Xcp/X max	Xcv/X max	$\Delta X/Lw$ (%)	CmG
$\delta = 7$ deg, $n = 0.7$	0.828	0.881	14.0	8.45^{E}-4
$\delta = 9$ deg, $n = 1.0$	0.864	0.901	11.0	8.94^{E}-4

2. Aerodynamic Stability

Waveriders are known to be statically unstable [10] that is, their center of pressure (where the aerodynamic resultant is applied) is upward of the center of gravity. The pitching moments of the optimized waveriders have been computed to evaluate their degree of instability. Only the lift is taken into account because of the small vertical distances making the drag work: there is a shift of two orders of magnitude between moments due to the lift and that due to the drag. The center of pressure is the point where the pitching moment is null. The center of pressure location (measured from zero, the body nose that is the origin of the frame) Xcp is equal to $-Moz/L$ (the moment at the point zero, Moz, is negative because of the z-axis orientation).

The center of volume is the center of gravity of the body considered as homogeneous. Its streamwise location, measured from zero, is Xcv. ΔX, the distance between the two centers, is equal to a certain percentage of the waverider length. It characterizes the degree of instability of the considered body. The waverider length relative to zero coincides with the base location, $Xbase$. Table 5 gives all these characteristics for the cases $\delta = 7$ deg, $n = 0.7$ and $\delta = 9$ deg, $n = 1.0$. The optimized waveriders are therefore unstable. The optimized $\delta = 9$ deg, $n = 1.0$ waverider is slightly less unstable than the $\delta = 7$ deg, $n = 0.7$ one (ΔX equal to, respectively, 11 and 14% of the waverider length). This can be explained by looking at the undersurface pressure distributions in Fig. 16. In the cone case, higher pressures are located just upstream of the base, whereas, with a convex power-law body, higher pressures are located close to the nose (see Fig. 15). Stability can be improved by designing upper surfaces that create an expansion just upstream of the base.

V. Conclusion

Power-law blunt body-derived waveriders have been studied in an attempt to improve both lift-to-drag ratio and volume. Small-disturbance theory showed its limits at Mach 5, which explains the use of a Euler code to create the flowfields. This last method has been well validated for cone-derived waveriders by a comparison with Taylor–Maccoll results. Nonuniformity of the external flowfield has negligible effect on the friction stresses. Influences of the parameters have been pictured in the particular case of parabolic-top cone-derived waveriders. In the case of more complex upper surfaces, a simplex-based method enabled us to optimize the viscous lift-to-drag ratio of waveriders having a thickness-to-length ratio equal to 0.1. It appears that the choice of a blunt body as a reference body rather than that of a simple cone generates a slight increase of the lift-to-drag ratio and a 20% rise for the volume of the waverider.

The method exposed here is therefore well adapted, for instance, for the optimization of an hypersonic glider that must carry a huge charge. The most simple examples of that are the bomb bay or weapon magazine of a military aircraft; but civil applications, like the first given in the Introduction, are also possible. The main result is that the conception of an easy-to-control, loaded hypersonic vehicle flying on large distances should be facilitated.

References

[1] Nonweiler, T. R. F., "Delta Wings of Shape Amenable to Exact Shock Wave Theory," *Journal of the Royal Aeronautical Society*, Vol. 67, No. 1, 1963, p. 39.

[2] Kuchemann, D., *The Aerodynamic Design of Aircraft*, Pergamon, Oxford, 1978, pp. 448–510.

[3] Corda, S., and Anderson, J. D., "Viscous Optimized Hypersonic Waveriders Designed from Axisymmetric Flowfields," AIAA Paper 88-0369, Jan. 1988.

[4] Bowcutt, K. G., Anderson, J. D., and Capriotti, D., "Viscous Optimized Hypersonic Waveriders," AIAA Paper 87-0272, 1987.

[5] Jacquotte, O. P., Montigny-Rannou, F., and Goussement, G., "Generation, Optimization and Adaptation of Multi-Block Structured Grids for Complex Configurations," *Survey on Mathematics for Industry*, Vol. 4, 1995, pp 267–277.

[6] Rasmussen, M. L., and Brandes-Duncan, B., "Hypersonic Waveriders Generated from Power-Law Shocks," AIAA Paper 95-6160, 1995.

[7] Péchier, M., "Prévisions Numériques de l'effet Magnus pour des Configurations de Munition," Ph.D. Dissertation, Department of Mechanical Engineering, Univ. of Poitiers, France, Sept. 1999.

[8] Mangin, B., Benay, R., and Chanetz, B., "Augmentation de la Finesse d'un Engin Hypersonique par Application du Concept Waveriders," DAFE ONERA-RT 5/08424, 2003.

[9] Zucrow, M. J., and Hoffman, J. D., *Gas Dynamics*, Vols. 1 and 2, Wiley, New York, 1976.

[10] Rasmussen, M. L., "Analysis of Cone-Derived Waveriders by Hypersonic Small-Disturbance Theory," *Proceedings of the 1st International Hypersonic Waverider Symposium*, NASA/Univ. of Maryland, Dept. of Aerospace Engineering, 1990.

[11] Kim, B. S., Rasmussen, M. L., and Jischke, M. C., "Optimization of Waverider Configurations Generated from Axisymmetric Conical Flows," *Journal of Spacecraft and Rockets*, Vol. 20, No. 5, 1983, pp. 461–469.

[12] Cousteix, J., *Turbulence et Couche Limite*, Cépadues-Éditions, Toulouse, France, 1989.

[13] Stainback, P. C., Wagner, R. D., Owen, F. K., and Horstman, C. C., "Experimental Studies of Hypersonic Boundary-Layer Transition and Effects of Wind-Tunnel Disturbances," NASA TND 7453, 1974.

[14] Nelder, J. A., and Mead, R., "A Simplex Method for Function Minimization," *Computer Journal (UK)*, Vol. 7, Jan. 1965, pp. 308–313.

[15] Anderson, J. D., Jr., *Hypersonic and High Temperature Gas Dynamics*, Series in Aeronautical and Aerospace Engineering, McGraw–Hill, New York, 1989.

[16] Lobbia, M., and Suzuki, K., "Design and Analysis of Payload-Optimized Waveriders," AIAA Paper 2001-1849, 2001.

M. Miller
Associate Editor